Z. Phys. C – Particles and Fields 40, 63–75 (1988)

Zeitschrift für Physik C Particles and Fields

Determination of quark and gluon vacuum condensates from τ-lepton decay data

C.A. Dominguez* and J. Solà**
Deutsches Elektronen-Synchrotron DESY, D-2000 Hamburg, Federal Republic of Germany

Received 23 November 1987

Abstract. The values of the gluon and four-quark vacuum condensates are estimated using recent experimental data on the semileptonic τ-lepton decays $\tau \to \nu_\tau + n\pi$, which determine the vector and axial-vector hadronic spectral functions. An optimal estimate is achieved through a systematic combined use of Finite Energy, Laplace and Gaussian transform QCD sum rules. As a byproduct, the values of the dimension $d = 8$ vacuum condensates in the vector and axial-vector channels are also estimated.

1 Introduction

The method of QCD sum rules, first introduced by Shifman et al. [1], has become a popular and powerful technique to study hadronic physics in the low energy resonance region [2]. As is well known, this method relates through dispersion relations low energy parameters, e.g. particle masses and coupling constants, to the Operator Product Expansion (OPE) of current correlators at short distances. The basic underlying assumption is that this OPE remains valid in the presence of non-perturbative effects which are parametrized by a set of vacuum expectation values of quark and gluon fields. These vacuum condensates induce power corrections to asymptotic freedom and are supposed to be responsible for the rich resonance structure observed at low energies [3]. To be more specific let us consider the following two-point function

$$\Pi(q^2) = i\int d^4x e^{iqx} \langle 0|T(J(x)J^\dagger(0))|0\rangle \qquad (1)$$

where $J(x)$ stands for any local current built from the quark and gluon fields appearing in the fundamental QCD Lagrangian. The corresponding OPE reads

$$i\int d^4x e^{iqx} T(J(x)J(0)) = C_0\hat{1} + \sum_N C_N(q)\hat{O}_N \qquad (2)$$

where the Wilson coefficients in this expansion depend on the Lorentz indices and quantum numbers of $J(x)$ and also of the local gauge invariant operators $\hat{O}_N$ built from quark and gluon fields. These operators are ordered by increasing dimensionality and the Wilson coefficients, calculable in perturbation theory, fall off by corresponding powers of q^2. The unit operator in (2) has dimension $d = 0$ and $C_0\hat{1}$ stands for the purely perturbative contribution. Examples of $d = 4$ operators are $m_q\bar{q}q$ and $G^a_{\mu\nu}G^a_{\mu\nu}$. To use the OPE (2) in (1) one assumes that short and long distance effects factorize. The former are buried in the Wilson coefficients and the later in the non-vanishing vacuum expectation values $\langle 0|\hat{O}_N|0\rangle$. After this the rest follows from analiticity, viz. $\Pi(q)$ satisfies a dispersion relation and thus one relates the hadronic spectral function appearing there to the OPE. Different choices of the weight in the dispersion relation lead to different kinds of QCD sum rules, e.g. Hilbert, Laplace or Gaussian transforms, Finite Energy Sum Rules (FESR), etc.

Concerning the actual numerical values of the various quark and gluon condensates, in general they cannot be computed from first principles as this would be tantamount to solving QCD exactly. Hence, the standard procedure has been to extract these condensates by using QCD sum rules in a few channels where experimental data on the hadronic spectral functions is available, e.g. the charmonium system [1, 4–7], e^+e^- cross sections [8–12] etc. Once the values of the various vacuum condensates are known one may proceed to apply the QCD sum rules to other channels and make predictions for particle masses, couplings constants, etc. Using experimental information on charmonium as well as on e^+e^- cross sections, some authors have found [1, 4–5, 8–9]

* Alexander von Humboldt Research Felow. On leave of absence from: Facultad de Física, Pontificia Universidad Católica de Chile, Santiago, Chile
** On leave from Department de Física, Universitat Autònoma de Barcelona, Barcelona, Catalonia

$$\frac{\pi}{3}\langle\alpha_s G^2\rangle \simeq 0{\cdot}04\,\text{GeV}^4 \tag{3}$$

which we shall refer to as the standard value of the gluon condensate. However, this result is somewhat controversial, to wit: it has been conjectured in the framework of potential models [13], as well as in two-dimensional QCD [14], that the value (1) may be an underestimate. Also, a value about 30% higher has been advocated in [2], and recent charmonium [6–7] and e^+e^- [11–12] analyses suggest even larger deviations. A separate controversy exists in connection with the vacuum saturation approximation [1] often used to estimate the magnitude of the dimension-six four-quark condensates, e.g.

$$\langle(\bar{q}\gamma_\mu\lambda^a q)^2\rangle|_{V.S} = -\frac{16}{9}\langle q\bar{q}\rangle^2 \tag{4}$$

where λ^a are the Gell-Mann matrices in colour space. In fact, several authors have noticed that this approximation leads to inconsistencies [9, 15–17] a view supported by some e^+e^- analyses [11, 12].

Given the impact of the gluon and the four-quark condensates on current phenomenology it becomes quite important to attempt a resolution of the above discrepancies. This should be done e.g. by using as many independent sets of experimental data as possible and, at the same time, employing different kinds of sum rules in a systematic fashion. In fact, depending on the choice of kernel in the dispersion relations the extraction of the vacuum condensates may be more or less sensitive to a given parametrization of the data, as well as to the influence of higher dimensional condensates.

In this paper we wish to present an attempt in this direction by exploiting the unique opportunity being offered by the availability of τ-lepton semileptonic decay data from the ARGUS collaboration at DORIS [18], namely $\tau \to \nu_\tau 2\pi$ and $\tau \to \nu_\tau 4\pi$ which determine, essentially, the vector isovector hadronic spectral function, and $\tau \to \nu_\tau \rho\pi$ which relates to the axial-vector isovector channel. These data have been used recently [19] to study the saturation of the Weinberg sum rules and to estimate the $\pi^\pm - \pi^0$ mass difference in QCD. Here we shall consider the vector and the axial-vector channels separately and extract the vacuum condensates from the corresponding sum rules. Since the gluon condensate contributes equally to both cases we shall be able to perform valuable consistency checks on our analysis. In order to optimize the determination of the vacuum condensates we shall make a systematic combined use of FESR, Laplace and Gaussian transform QCD sum rules.

The paper is organized as follows. In Sect. 2 we define the two-point functions for the vector and axial-vector channels and give their QCD expressions. The various types of QCD sum rules are introduced in Sect. 3, where we also discuss briefly their advantages and shortcomings. In Sect. 4 we present the various numerical fits to the experimental data. Sections 5, 6 and 7 contain the results obtained from the FESR, Laplace and Gaussian transforms, respectively. In Sect. 8 we discuss the impact of higher dimensional condensates concentrating on the dimension $d = 8$. Finally, in Sect. 9 we summarize our results.

2 Two-point functions and the *OPE* in *QCD*

We start by defining the two-point function

$$\Pi^{VV}_{\mu\nu}(q^2) = i\int d^4x e^{iqx}\langle 0|\,T(V_\mu(x)V^\dagger_\nu)(0)|0\rangle \tag{5}$$

where the current $V_\mu(x)$ has the quantum numbers of the ρ-meson, i.e.

$$V_\mu(x) = \tfrac{1}{2}[\bar{u}(x)\gamma_\mu u(x) - \bar{d}(x)\gamma_\mu d(x)]. \tag{6}$$

From the conservation of the vector current one can write

$$\Pi^{VV}_{\mu\nu}(q^2) = -(g_{\mu\nu}q^2 - q_\mu q_\nu)\Pi_V(q^2). \tag{7}$$

The function $\Pi_V(q^2)$ in (7) has been calculated in perturbation theory, in the $\overline{MS}$ renormalization scheme [20], up to three loops [21], and including the leading non-perturbative corrections [1], with the result ($Q^2 \equiv -q^2 > 0$)

$$\begin{aligned}8\pi^2\Pi_V(q^2) = &-\ln\frac{Q^2}{\nu^2} + \frac{5}{3} - \frac{3}{Q^2}[m_u^2(\nu^2) + m_d^2(\nu^2)] \\ &- \frac{\alpha_s(\nu^2)}{\pi}\ln\frac{Q^2}{\nu^2} + \left[\frac{\alpha_s(\nu^2)}{\pi}\right]^2 \\ &\cdot\left[\frac{-\beta_1}{4}\ln^2\frac{Q^2}{\nu^2} - F_3\ln\frac{Q^2}{\nu^2}\right] \\ &+ \frac{C_4\langle O_4\rangle_V}{Q^4} + \frac{C_6\langle O_6\rangle_V}{Q^6} + \frac{C_8\langle O_8\rangle_V}{Q^8} \\ &+ \mathcal{O}\left(\frac{m_q^4}{Q^4}\right) + \mathcal{O}\left[\left(\frac{\alpha_s}{\pi}\right)^3\right] + \mathcal{O}\left(\frac{1}{Q^{10}}\right)\end{aligned} \tag{8}$$

where $\beta_1 = -29/6$ and $F_3 = 1.756\ldots$ for three colours and two flavours.

The non-perturbative term of dimension $d = 4$ is given by

$$C_4\langle O_4\rangle_V = \frac{\pi}{3}\langle\alpha_s G^2\rangle + 4\pi^2[m_u\langle\bar{u}u\rangle + m_d\langle\bar{d}d\rangle] \tag{9}$$

In principle there are various operators contributing to $C_6\langle O_6\rangle$, namely the quark-gluon, the three gluon and the four-quark condensates. The first is suppressed by a factor of m_q^2 [1–2], while the second gives no contribution in the case of light quarks [22–23], thus leaving only the four-quark condensate contribution

$$\begin{aligned}C_6\langle O_6\rangle_V = &-8\pi^3\alpha_s[\langle(\bar{q}\gamma_\mu\gamma_5\lambda^a q)^2\rangle \\ &+ \tfrac{2}{9}\langle(\bar{q}\gamma_\mu\lambda^a q)^2\rangle]\end{aligned} \tag{10}$$

There are quite a few quark and gluon condensates

contributing to $C_8\langle O_8\rangle$. The Wilson coefficients of the various condensates for light quark currents have been computed in [24]. We defer a discussion on $C_8\langle O_8\rangle$ till Sect. 8 and proceed with our analysis neglecting this term. We shall also neglect the quark mass loop insertion term proportional to m_q^2 in eq. (8) as it has no impact on our results. We shall retain, however, the second term in (9) which may be estimated using the well known current algebra low energy theorem [25]

$$-(m_u+m_d)\langle\bar{u}u+\bar{d}d\rangle=2f_\pi^2\mu_\pi^2(1-\delta_\pi) \tag{11}$$

where δ_π stands for the (analytic) corrections to pion-PCAC. These corrections have been estimated through QCD sum rules in the pionic channel [26–27]: $\delta_\pi=(4\pm1)\%$. Assuming $\langle\bar{u}u\rangle\simeq\langle\bar{d}d\rangle$ one finds from (11)

$$4\pi^2[m_u\langle\bar{u}u\rangle+m_d\langle\bar{d}d\rangle]\simeq-0.0064\,\mathrm{GeV}^4. \tag{12}$$

In this way and with Λ_{QCD} fixed, e.g. $\Lambda_{\mathrm{QCD}}=100$ MeV, (8) contains as free parameters the gluon condensate and the four-quark condensate (eventually also the $d=8$ condensates) which we shall determine by confronting (8) with the $\tau\to\nu_\tau 2\pi$ and $\tau\to\nu_\tau 4\pi$ data. The reference value for $\langle\alpha_s G^2\rangle$ was given in (3). In the case of $C_6\langle O_6\rangle$ we could take as reference value the one following from the vacuum saturation approximation [1]. Making use of the relation [1]

$$\langle(\bar{q}\gamma_\mu\gamma_5\lambda^a q)^2\rangle|_{\mathrm{v.s.}}=-\langle(\bar{q}\gamma_\mu\lambda^a q)^2\rangle|_{\mathrm{v.s.}} \tag{13}$$

together with (4) in (10) one finds [1]

$$C_6\langle O_6\rangle_V|_{\mathrm{v.s.}}=-\tfrac{896}{81}\pi^3\alpha_s\langle\bar{q}q\rangle^2\simeq-0.06\,\mathrm{GeV}^6. \tag{14}$$

Turning to the axial-vector channel we define

$$\begin{aligned}\Pi_{\mu\nu}^{AA}(q^2)&=i\int d^4x e^{iqx}\langle 0|T(A_\mu(x)A_\nu^\dagger(0))|0\rangle\\&=-g_{\mu\nu}\tilde{\Pi}_A(q^2)+q_\mu q_\nu\Pi_A(q^2)\end{aligned} \tag{15}$$

where the current $A_\mu(x)$ has the quantum numbers of the A_1-meson, i.e.

$$A_\mu(x)=\tfrac{1}{2}[\bar{u}(x)\gamma_\mu\gamma_5 u(x)-\bar{d}(x)\gamma_\mu\gamma_5 d(x)]. \tag{16}$$

Since $A_\mu(x)$ is not conserved (15) contains two independent structure functions. However, at large $Q^2\equiv-q^2$ and to leading order in the quark masses one has the relation [1]

$$\tilde{\Pi}_A(Q^2)+Q^2\Pi_A(Q^2)=\frac{(m_u+m_d)\langle\bar{u}u+\bar{d}d\rangle}{Q^2}. \tag{17}$$

Concentrating on e.g. $\Pi_A(q^2)$, its perturbative QCD expression is the same as that for $\Pi_V(q^2)$ in (8). However, the non-perturbative coefficients are different, viz.

$$C_4\langle O_4\rangle_A=\frac{\pi}{3}\langle\alpha_s G^2\rangle-4\pi^2[m_u\langle\bar{u}u\rangle+m_d\langle\bar{d}d\rangle] \tag{18}$$

$$C_6\langle O_6\rangle_A=-\tfrac{88}{9}\pi^3\alpha_s\langle(\bar{q}\gamma_\mu\lambda^a q)^2\rangle. \tag{19}$$

Notice that $C_4\langle O_4\rangle_A$ should be larger than $C_4\langle O_4\rangle_V$ by precisely twice the value (12), i.e.

$$C_4\langle O_4\rangle_A-C_4\langle O_4\rangle_V\simeq0.013\,\mathrm{GeV}^4 \tag{20}$$

On the other hand, comparing eqs. (10) and (19) and using (13) one finds

$$\left.\frac{C_6\langle O_6\rangle_A}{C_6\langle O_6\rangle_V}\right|_{\mathrm{v.s.}}=-\frac{11}{7}. \tag{21}$$

These two relations will become useful later on to perform valuable consistency checks on the results of our analysis. Concerning $C_8\langle O_8\rangle_A$, at least the contribution from the gluonic operators should be the same as in $C_8\langle O_8\rangle_V$ as calculated in [24].

3 QCD sum rules

3.1 Finite energy sum rules

Finite Energy Sum Rules (FESR), including radiative corrections to order $\mathcal{O}(\alpha_s^2)$, have been derived in [10]. For the vector or the axial-vector channel they read

$$\begin{aligned}C_{4N+2}\langle O_{4N+2}\rangle_{V,A}&=8\pi^2\int_0^{s_0}ds s^{2N}\frac{1}{\pi}\mathrm{Im}\,\Pi_{V,A}(s)\\&\quad-\frac{s_0^{2N+1}}{2N+1}[1+F_{4N+2}(s_0)]\end{aligned} \tag{22}$$

$$\begin{aligned}-C_{4N+4}\langle O_{4N+4}\rangle_{V,A}&=8\pi^2\int_0^{s_0}ds s^{2N+1}\frac{1}{\pi}\mathrm{Im}\,\Pi_{V,A}(s)\\&\quad-\frac{s_0^{2N+2}}{2N+2}[1+F_{4N+4}(s_0)]\end{aligned} \tag{23}$$

where $N=0,1,2,\ldots$, and the radiative corrections $F_p(s_0)$, with $p=4N+2$ or $p=4N+4$, are given by

$$F_p(s_0)=\frac{\alpha_s(s_0)}{4}+\left[\frac{\alpha_s(s_0)}{\pi}\right]^2\left(F_3-\frac{\beta_1}{p}-\frac{\beta_2}{\beta_1}\ln\ln\frac{s_0}{\Lambda_{\mathrm{QCD}}^2}\right) \tag{24}$$

where F_3 and β_1 were defined previously (8), $\beta_2=-115/12$ for three colours and two flavours, and

$$\frac{\alpha_s(s_0)}{\pi}=\frac{2}{-\beta_1\ln(s_0/\Lambda_{\mathrm{QCD}}^2)}. \tag{25}$$

In the above equations s_0 is the threshold for asymptotic freedom, i.e, for $s>s_0$ the spectral function behaves as predicted by perturbative QCD. Since the quark mass loop insertion term in eq. (8), formally equivalent to a $C_2\langle O_2\rangle$ effective contribution, is negligible one finds from (22) with $N=0$

$$1+F_2(s_0)\equiv I_0(s_0)|_{V,A}=\frac{8\pi^2}{s_0}\int_0^{s_0}ds\frac{1}{\pi}\mathrm{Im}\,\Pi_{V,A}(s). \tag{26}$$

Hence, in this case s_0 is not a free parameter to be determined from additional physical assumptions outside the sum rule framework, but rather it is a solution of the above eigenvalue equation. Once s_0 is deter-

mined from (26) one may proceed to determine the values of $C_N\langle O_N\rangle$ using the remaining (22)–(23).

There is an important issue, often overlooked in past applications of these sum rules, which has to do with the stability of the eigenvalue solutions to the FESR. As first pointed out in [28] one should trust predictions from FESR provided they are stable against reasonable changes of s_0 inside some duality region; only then there will be duality between the experimental data and a given set of QCD parameters. One expects that the more accurate the parametrization of the data the wider this duality region where e.g. the rhs of (26) will be approximately equal to its lhs. A wide duality region seems to guarantee the stability of the vacuum condensates [10, 11, 27–29], at least for those of lowest dimension. Clearly, the power-like weight of the spectral function in the FESR will eventually be the cause of their failure in making reliable predictions for high dimensional condensates. That this stability issue is not trivial may be seen by parametrizing e.g. the vector or the axial-vector spectral function with a delta function. In this case the slowly varying lhs of (26) will intercept the rapidly varying rhs at only one point. The duality region then reduces to a single value of s_0 and, furthermore, the vacuum condensates extracted from (22)–(23) turn out to be quite unstable against small changes around this eigenvalue. As shown in [11], in connection with the vector case, this instability problem does not get any better by attempting a finite-width single resonance parametrization of the spectral function. It is only when a fit to the actual e^+e^- data is used in the FESR that one finds stable eigenvalue solutions.

3.2 Laplace transform sum rules

Another useful set of QCD sum rules is that based on the Laplace transform of the spectral function [1]

$$L(\sigma)=\int_0^\infty ds e^{-s\sigma}\frac{1}{\pi}\operatorname{Im}\Pi(s) \tag{27}$$

where the Laplace variable σ plays now the role of the short distance expansion parameter analogous to $1/Q^2$ in e.g. (8). In the case of vector or axial-vector current correlators the QCD expression for $L(\sigma)$ reads [30]

$$\begin{aligned}8\pi^2\sigma L_{V,A}(\sigma)=1+\frac{\alpha_s(1/\sigma)}{\pi}+\left[\frac{\alpha_s(1/\sigma)}{\pi}\right]^2&\cdot\left[F_3-\tfrac{1}{2}\beta_1\gamma_E+\frac{\beta_2}{\beta_1}\ln\ln(\sigma\Lambda^2)\right]\\&+C_4\langle O_4\rangle_{V,A}\sigma^2+C_6\langle O_6\rangle_{V,A}\cdot\frac{\sigma^3}{2!}+C_8\langle O_8\rangle_{V,A}\frac{\sigma^4}{3!}\\&+\mathcal{O}(m_q^2\sigma^2)+\mathcal{O}\left[\left(\frac{\alpha_s}{\pi}\right)^3\right]+\mathcal{O}(\sigma^5)\end{aligned} \tag{28}$$

where $\gamma_E=0.5772\ldots$ is the Euler constant.

Because of its exponential weight, the Laplace transform (27) places more emphasis on the low energy part of the hadronic spectral function, a clear advantage over e.g. the FESR. At the same time, however, the influence of s_0 becomes exponentially suppressed and, hence, for all practical purposes s_0 ends up as an adjustable parameter not fixed by the Laplace sum rules themselves. On the QCD side, higher dimensional condensates become factorially suppressed. Since our knowledge of the Wilson coefficients does not usually go beyond $d=8$, this feature appears as an advantage. Nevertheless, notice from (28) that now *all* of the condensates appear in the sum rules; it might happen in some cases that the factorial suppression may not be enough to quench some of the higher dimensional condensates. As we shall discuss in more detail later (cf. Sect. 6) this fact can make it difficult to extract the values of $C_N\langle O_N\rangle$ in an unbiased way. In contrast, vacuum condensates of different dimensionality obey *uncoupled* FESR, at least when no radiative corrections are taken into account in the Wilson coefficients (for a generalization to higher orders in α_s see [31]).

In practical applications of Laplace transform QCD sum rules it has been customary to consider the ratio

$$R(\sigma)\equiv\frac{L'(\sigma)}{L(\sigma)}=\frac{\int_0^\infty ds e^{-s\sigma}s\frac{1}{\pi}\operatorname{Im}\Pi(s)}{\int_0^\infty ds e^{-s\sigma}\frac{1}{\pi}\operatorname{Im}\Pi(s)} \tag{29}$$

where $L'(\sigma)$ stands for $dL(\sigma)/d\sigma$. On the hadronic side the ratio (29) tends to minimize the experimental errors in the spectral function while on the QCD side it tends to emphasize the non-perturbative contributions over the purely perturbative ones, viz.

$$R(\sigma)|_{\mathrm{QCD}}=\left(\frac{1}{\sigma}\right)\frac{1+F_L(\sigma)-C_4\langle O_4\rangle\sigma^2-C_6\langle O_6\rangle\sigma^3-\frac{1}{2}C_8\langle O_8\rangle\sigma^4+\cdots}{1+F_L(\sigma)+C_4\langle O_4\rangle\sigma^2+\frac{1}{2}C_6\langle O_6\rangle\sigma^3+\frac{1}{3!}C_8\langle O_8\rangle\sigma^4+\cdots} \tag{30}$$

where $F_L(\sigma)$ stands for the perturbative terms in eq. (28). We shall adhere to this established practice and use the ratio (29) in our analysis.

3.3 Gaussian sum rules

The final set of sum rules we will consider is that based on the Gaussian transform of the spectral function [10]

$$G(\hat{s},\tau)=\frac{1}{\sqrt{4\pi\tau}}\int_0^\infty ds e^{-(s-\hat{s})^2/4\tau}\frac{1}{\pi}\operatorname{Im}\Pi(s) \tag{31}$$

i.e. the convolution of the spectral function with a Gaussian kernel centered at an arbitrary point $\hat{s}$ with a finite-width resolution $\sqrt{4\tau}$. The short distance expansion parameter in this case is $1/\sqrt{4\tau}$, while $\sqrt{4\tau}$ determines the resolution with which the physical spectrum is to be sampled at the various points $\hat{s}$. In

particular, for $\tau = 0$ one would obtain strict local duality, i.e.

$$G(\hat{s}, 0) = \frac{1}{\pi} \mathrm{Im}\, \Pi(\hat{s}) \tag{32}$$

However, this is only a hypothetical limit as it would imply a complete solution to the bound state problem in QCD. Therefore, in practice τ must be kept finite, typically $\tau \simeq 0.5$–$1.5\,\mathrm{GeV}^4$ [10–11, 27–29]. A very important property of $G(\hat{s}, \tau)$ is that it obeys the partial differential equation

$$\frac{\partial^2 G(\hat{s}, \tau)}{(\partial \hat{s})^2} = \frac{\partial G(\hat{s}, \tau)}{\partial \tau} \tag{33}$$

which is nothing but the heat equation if one reinterprets $\hat{s}$ as a 'position' variable and τ as a 'time' variable. In this analogy the hadronic spectral function corresponds to the initial heat distribution in a semi-infinite rod $0 \leqq \hat{s} \leqq \infty$ and $G(\hat{s}, \tau)$ measures the evolution in time of the heat distribution in this rod. This provides a convenient framework to check the consistency between given data on the spectral function and a specific choice of QCD parameters, e.g. Λ_{QCD}, s_0 and the values of the vacuum condensates in the OPE. In fact, after a certain 'time' τ sufficiently large so that the uncalculated QCD corrections become relatively small, the predicted QCD heat distribution should match the evolution of the data. This is the heat evolution test first proposed in [10] and which serves as a quantitative formulation of the notion of local duality.

The heat equation (33) for the semi-infinite rod $0 \leqq \hat{s} \leqq \infty$ admits two general solutions corresponding to the two possible choices of boundary conditions: vanishing function or vanishing first partial derivative with respect to $\hat{s}$ at the origin, both for $\tau > 0$, subject to the initial condition (32). Denoting these two solutions by $U^-(\hat{s}, \tau)$ and $U^+(\hat{s}, \tau)$, respectively, one has

$$U^+(\hat{s}, \tau) = G(\hat{s}, \tau) + G(-\hat{s}, \tau) \tag{34}$$

$$U^-(\hat{s}, \tau) = G(\hat{s}, \tau) - G(-\hat{s}, \tau), \tag{35}$$

The calculation of $U^{\pm}(\hat{s}, \tau)$ in QCD has been discussed in [10] and the result is

$$\begin{aligned} 8\pi^2 U^+_{V,A}(\hat{s}, \tau) &= 1 + \frac{\alpha_s(\sqrt{\tau})}{\pi} + \left[\frac{\alpha_s(\sqrt{\tau})}{\pi}\right]^2 \left\{\left[F_3 - \frac{\beta_2}{\beta_1} \ln\ln \frac{\sqrt{\tau}}{\Lambda^2_{\mathrm{QCD}}}\right] \right. \\ &\left. + \beta_1 \left[\int_0^{\hat{x}} dz\, D(z) - \frac{\gamma_E}{4}\right]\right\} + \mathcal{O}\left\{\left[\frac{\alpha_s(\sqrt{\tau})}{\pi}\right]^3\right\} \\ &+ \frac{2}{\sqrt{\pi}} e^{-\hat{x}^2} \left[\mathcal{O}(m_q^2/\sqrt{\tau}) \right. \\ &\left. + \frac{1}{2} \frac{C_6 \langle O_6 \rangle_{V,A}}{(2\sqrt{\tau})^3} H_2(\hat{x}) + \cdots\right] \end{aligned} \tag{36}$$

$$\begin{aligned} 8\pi^2 U^-_{V,A}(\hat{s}, \tau) &= erf(\hat{x}) \left\{1 + \frac{\alpha_s(\sqrt{\tau})}{\pi} + \left[\frac{\alpha_s(\sqrt{\tau})}{\pi}\right]^2 \right. \\ &\cdot \left[F_3 + \frac{\beta_1}{2} \ln 2 - \tfrac{1}{4}\beta_1 \gamma_E \right. \\ &\left. \left. - \frac{\beta_2}{\beta_1} \ln\ln \frac{\sqrt{\tau}}{\Lambda^2_{\mathrm{QCD}}}\right]\right\} + \left[\frac{\alpha_s(\sqrt{\tau})}{\pi}\right]^2 \\ &\cdot \beta_1 \int_0^{\hat{x}} dz\, Der\, f(z) + \mathcal{O}\left\{\left[\frac{\alpha_s(\sqrt{\tau})}{\pi}\right]^3\right\} \\ &+ \frac{2}{\sqrt{\pi}} e^{-\hat{x}^2} \left[- \frac{C_4 \langle O_4 \rangle_{V,A}}{4\tau} H_1(\hat{x}) \right. \\ &\left. - \frac{C_8 \langle O_8 \rangle_{V,A}}{96\tau^2} H_3(\hat{x}) - \cdots\right] \end{aligned} \tag{37}$$

where

$$\hat{x} \equiv \frac{\hat{s}}{2\sqrt{\tau}}, \tag{38}$$

$erf(\hat{x})$ is the error function, $H_n(\hat{x})$ are Hermite polynomials,

$$D(z) = e^{-z^2} \int_0^z dt\, e^{t^2} \tag{39}$$

is the Dawson function,

$$Der\, f(z) = e^{-z^2} \int_0^z dt\, e^{t^2} erf(t), \tag{40}$$

and $\alpha_s(\sqrt{\tau})$ is given as in (25).

Notice that $U^+(\hat{s}, \tau)$ contains the dimension $d = 6$ vacuum condensate (and eventually $d = 10$, etc. which we are not considering here), while $U^-(\hat{s}, \tau)$ contains $C_4\langle O_4\rangle$ and $C_8\langle O_8\rangle$. This will allow for two independent heat evolution tests to be performed on the eigenvalue solutions to the FESR, as well as on the results from the Laplace transform analysis.

3.4 Comparative discussion of the QCD sum rules

It should be clear from our short review of the various QCD sum rules above that each one of them has advantages as well as shortcomings. A brief summary follows.

(i) Because of their exponential kernel the Laplace transform QCD sum rules emphasize the low energy, ground state, part of the hadronic spectral function. Therefore, an accurate knowledge of the data in the intermediate and high energy region may not be necessary. In contrast, FESR are rather sensitive to this region and hence call for a much more accurate parametrization of the data.

(ii) In spite of the Laplace factorial suppression of higher dimensional non-perturbative terms in the OPE, this might not be enough to avoid a biased determination of the lowest dimensional condensates through a confrontation between (29) and (30). To

elaborate on this point suppose we assume that $C_6\langle O_6\rangle = C_8\langle O_8\rangle = \cdots = 0$ and then proceed to determine $C_4\langle O_4\rangle$ by fitting $R(\sigma)|_{QCD}$ in (30) to $R(\sigma)|_{DATA}$ in (29). Let us call this result $C_4\langle O_4\rangle|_1$. In a second step we take into account $C_4\langle O_4\rangle$ and $C_6\langle O_6\rangle$ but continue to neglect $C_8\langle O_8\rangle$, etc., and call these results $C_4\langle O_4\rangle|_2$ and $C_6\langle O_6\rangle|_1$. If $C_6\langle O_6\rangle$ is not negligible we would expect in general $C_4\langle O_4\rangle|_1 \neq C_4\langle O_4\rangle|_2$. In fact, as will be shown in Sect. 6 even the sign of $C_4\langle O_4\rangle|_2$ turns out to be different from that of $C_4\langle O_4\rangle|_1$. The established practice has been to stop the analysis at this second stage, assuming the influence of $C_8\langle O_8\rangle$ on $C_4\langle O_4\rangle|_2$ and $C_6\langle O_6\rangle|_1$ to be negligible. We shall argue later (cf. Sect. 8) that this may not be the case. At any rate, this Laplace correlation among the various vacuum condensates is absent in the FESR as they obey uncoupled eigenvalue equations, provided the corresponding Wilson coefficients are computed to lowest order in α_s (see [31]).

(iii) The value of the asymptotic freedom threshold s_0 is essentially a free parameter not fixed by the Laplace sum rules. In contrast, s_0 is one of the eigenvalue solutions to the FESR. However, the dependence of the vacuum condensates on s_0 is power-like in the FESR while it is exponentially quenched in Laplace sum rules.

(iv) Having fixed s_0 by means of some external arguments, predictions from Laplace sum rules follow from the criterion that there should exist some 'window' in σ such that perturbative QCD remains valid and, at the same time, only the leading power corrections are needed. This criterion should be thoroughly tested and checked by comparing with the results from the FESR. Nevertheless, the latter may only be trusted if the eigenvalue solutions are stable against changes in s_0 inside the duality window. The ultimate overall consistency check of whether the values of s_0 and of $C_N\langle O_N\rangle$ so determined are dual to the data or not, should be performed using the heat evolution tests which follow from the Gaussian sum rules.

Our conclusion is that Laplace transform and Finite Energy QCD sum rules are *complementary* tools to be used in the determination of the vacuum condensates. A systematic and reliable analysis should be based on both approaches together with the heat evolution tests. This is, in fact, the procedure we follow in the sequel to extract the QCD vacuum condensates from the τ-lepton decay data.

4 Fits to the data

The amplitude for the semileptonic decay of the τ-lepton into a non-strange ($S=0$) hadronic final state is given, in the four-Fermi approximation, by

$$A(\tau^{\pm} \to \nu_\tau + \text{hadrons}(S=0)) = \sqrt{2} G_F \cos\theta_c \bar{u}(p_{\nu_\tau}) \gamma^\mu (1-\gamma_5) u(p_\tau) \times \langle \text{hadrons}(S=0)| J_\mu^{1+i2} |0\rangle, \quad (41)$$

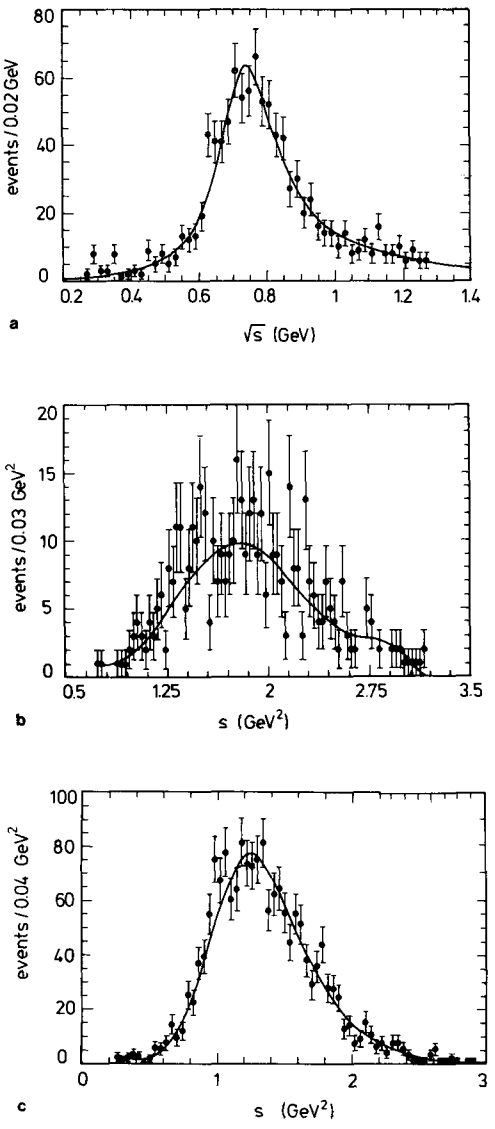

Fig. 1. a Experimental values of the invariant mass distribution for $\tau^{\pm} \to \nu_\tau \pi^{\pm} \pi^0$, together with the best fit to these data (solid curve). **b** Experimental values of the invariant mass distribution for $\tau^{\pm} \to \nu_\tau \pi^{\pm} \pi^+ \pi^- \pi^0$, together with the best fit to these data (solid curve). **c** Experimental values of the invariant mass distribution for $\tau^{\pm} \to \nu_\tau \rho^0 \pi^{\pm}$, together with the best fit to these data (solid curve)

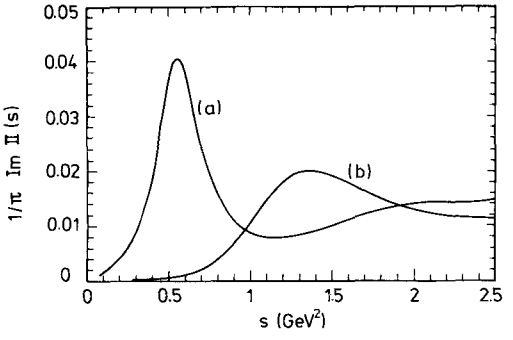

Fig. 2. Total hadronic spectral functions in the vector (curve a) and the axial-vector (curve b) channels. The pion-pole contribution to the latter is not shown

where $J_\mu^\alpha = V_\mu^\alpha - A_\mu^\alpha$. If the hadronic final state consists of an even (odd) number of pions then only the vector (axial-vector) piece of J_μ^α contributes to the matrix element in the rhs of (41). Therefore, the differential transition probabilities per invariant mass squared $d\Gamma/ds$ for the processes $\tau \to \nu_\tau + n\pi$ are related to the vector or axial-vector spectral functions, viz.

$$\sum_n \frac{d\Gamma(\tau \to \nu_\tau + n\pi)}{ds} = \frac{G_F^2 \cos^2\theta_c}{8\pi} \frac{1}{M_\tau^3}(M_\tau^2 + 2s)(M_\tau^2 - s)^2 \cdot \begin{cases} \frac{1}{\pi}\mathrm{Im}\,\Pi_V(s) & (n = \text{even}) \\ \frac{1}{\pi}\mathrm{Im}\,\Pi_A(s) & (n = \text{odd}). \end{cases} \tag{42}$$

In the axial-vector case the spectral function contains in addition the pion-pole which we treat separately.

Our analysis is based mainly on the recent data obtained by the ARGUS collaboration at DORIS [18]. The experimental invariant mass distributions for $\tau^\pm \to \nu_\tau \pi^\pm \pi^0$ and $\tau^\pm \to \nu_\tau \pi^\pm \pi^+ \pi^- \pi^0$ are shown in Fig. 1a and b, respectively. We also show there (solid curves) the result of the fits done in [19] using the product of a Breit–Wigner function with a high order polynomial (Fig. 1a) and a single high order polynomial (Fig. 1b). These fits were performed using the numerical program MINUIT and their quality is quite good as measured by the resulting values of the chi-squared per degree of freedom (χ_F^2), namely: $\chi_F^2 = \chi^2/51 = 0.89$ for Fig. 1a and $\chi_F^2 = \chi^2/81 = 0.76$ for Fig. 1b. Concerning the decay mode $\tau \to \nu_\tau \pi^\pm \pi^0 \pi^0 \pi^0$ we use the theoretical estimate of [32] based on CVC

$$\frac{\Gamma(\tau^\pm \to \nu_\tau \pi^\pm \pi^0 \pi^0 \pi^0)}{\Gamma(\tau^\pm \to \nu_\tau \pi^\pm \pi^+ \pi^- \pi^0)} = \frac{1}{5}. \tag{43}$$

As to higher multiplicity final states, e.g. $\tau \to \nu_\tau + 6\pi$, although there is no precise data available their contribution is thought to be negligible [32–33].

Finally, in order to obtain the vector spectral function through (42) we have used, as in [19],

$$\mathrm{BR}(\tau^\pm \to \nu_\tau \pi^\pm \pi^0) \simeq \mathrm{BR}(\tau^\pm \to \nu_\tau \rho^\pm) = (22.3 \pm 0.6 \pm 1.4)\% \tag{44}$$

and

$$\mathrm{BR}(\tau^\pm \to \nu_\tau \pi^\pm \pi^+ \pi^- \pi^0) = (4.5 \pm 0.4 \pm 1.5)\%. \tag{45}$$

The final result for $(1/\pi)\mathrm{Im}\,\Pi_V(s)$ is shown in Fig. 2 (curve a). We have found that the area under this spectral function is in excellent agreement with the area under the corresponding vector spectral function obtained from a fit to the e^+e^- data [11], as expected from CVC considerations. This agreement holds over a wide region of s extending up to $s \simeq 2.5\,\mathrm{GeV}^2$, which is quite enough for our purposes.

Turning to the axial-vector channel, the experimental invariant mass distribution for $\tau^\pm \to \nu_\tau \rho^0 \pi^\pm$ is shown in Fig. 1c. The solid curve in this figure is the result of the best chisquared fit performed with a Breit–Wigner function times a high order polynomial [19]. The resulting value of χ_F^2 is $\chi_F^2 = \chi^2/69 = 0.97$. There is no experimental information available in the channel $\tau^\pm \to \nu_\tau \rho^\pm \pi^0$. However, given the rather strong A_1-resonance dominance in $\tau^\pm \to \nu_\tau \rho^0 \pi^\pm$ (cf. [18, 34]) we can safely estimate the contribution of the former using isospin symmetry which simply entails $\mathrm{BR}(\tau^\pm \to \nu_\tau \rho^\pm \pi^0) = \mathrm{BR}(\tau^\pm \to \nu_\tau \rho^0 \pi^\pm)$. As with $\tau \to \nu_\tau 6\pi$ we shall neglect here the channel $\tau \to \nu_\tau 5\pi$.

A source of uncertainty in the extraction of $\mathrm{Im}\,\Pi_A$ from $d\Gamma/ds$ is due to the wide spread of experimental values for the branching ratio $\mathrm{BR}(\tau^\pm \to \nu_\tau \rho^0 \pi^\pm)$ [33, 35]. We shall use here the world average [33, 35]

$$\mathrm{BR}(\tau^\pm \to \nu_\tau \rho^0 \pi^\pm) = (6.6 \pm 0.6)\%. \tag{46}$$

In addition, there may be a non-negligible background contribution to the decay $\tau \to \nu_\tau + 3\pi$, i.e. [33–35]

$$\mathrm{BR}(\tau \to \nu_\tau + 3\pi)|_{\text{Non-Res.}} \leqq 1.4\%. \tag{47}$$

We have used here a very simple parametrization of this background in terms of $\varepsilon\pi$ non-resonant phase space normalized to the value (47). The final result for the axial-vector spectral function is shown in Fig. 2 (curve b). Not shown there, of course, is the pion-pole contribution which in the chiral limit is given by

$$\frac{1}{\pi}\mathrm{Im}\,\Pi_A(s)|_\pi = f_\pi^2 \delta(s), \tag{48}$$

where $f_\pi \simeq 93.2\,\mathrm{MeV}$.

Before closing this section we point out that to the hadronic parametrizations of the spectral functions discussed above one should add the perturbative QCD piece starting at some threshold s_0, viz.

$$\frac{1}{\pi}\mathrm{Im}\,\Pi_{V,A}(s) = \frac{1}{\pi}\mathrm{Im}\,\Pi_{V,A}(s)|_{\text{had.}} + \theta(s - s_0)\frac{1}{8\pi^2}\left[1 + \frac{\alpha_s}{\pi} + \cdots\right]. \tag{49}$$

5 Vacuum condensates from *FESR*

Using the fit to the vector spectral function discussed in Sect. 4 we have solved first the eigenvalue equation (26) to find the duality region. In Fig. 3 we plot the behaviour of the lhs of (26) (curve (b)) versus s_0. The solid curve (a) shows the corresponding behaviour of the rhs of (26). The duality region lies in the range

$$1.44\,\mathrm{GeV}^2 \leqq s_0 \leqq 1.75\,\mathrm{GeV}^2 \tag{50}$$

Solving next the FESR (22)–(23) for values of s_0 inside this region we find for $C_4\langle O_4\rangle_V$ and $C_6\langle O_6\rangle_V$ the results shown in Fig. 4 as curves (a) and (b), res-

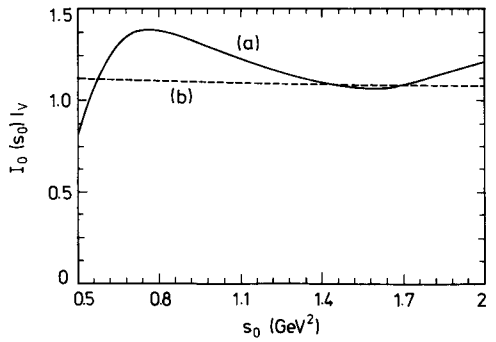

Fig. 3. Behaviour of the hadronic integral in the rhs of the FESR (26) (curve a) together with the behaviour of the QCD lhs (curve b), in the vector channel

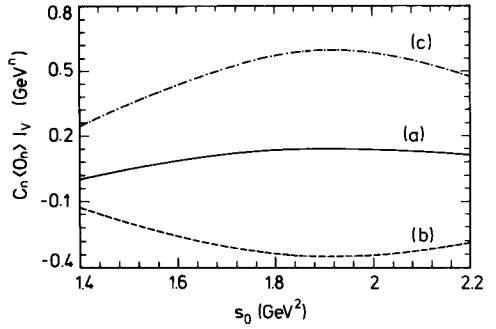

Fig. 4. Behaviour of $C_4\langle O_4\rangle_V$ (curve a), $C_6\langle O_6\rangle_V$ (curve b), and $C_8\langle O_8\rangle_V$ (curve c) as obtained from the FESR (22)–(23) in the vector channel

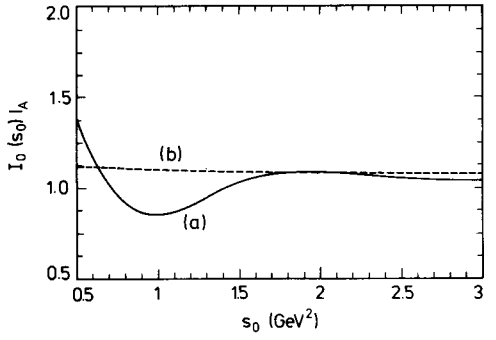

Fig. 5. Behaviour of the hadronic integral in the rhs of the FESR (26) (curve a) together with the behaviour of the QCD lhs (curve b), in the axial-vector channel

pectively. Also shown there (curve (c)) is the calculated behaviour of $C_8\langle O_8\rangle$, but we defer the discussion on this condensate till Sect. 8. As it may be appreciated from Fig. 4 the vacuum condensates are reasonably stable against changes in s_0 within the duality region. Numerically the results are

$$C_4\langle O_4\rangle_V = (0.025 - 0.11)\,\mathrm{GeV}^4 \tag{51}$$

$$C_6\langle O_6\rangle_V = -(0.16 - 0.32)\,\mathrm{GeV}^6. \tag{52}$$

Using (9) and (12) the above value of $C_4\langle O_4\rangle_V$ translates into

$$\frac{\pi}{3}\langle\alpha_s G^2\rangle = (0.03 - 0.12)\,\mathrm{GeV}^4. \tag{53}$$

This result is consistent with the standard value (3) as well as with higher values from other analysis [11–12]. However, it is barely consistent with a recent s-wave charmonium determination (cf. [7]) giving $(\pi/3)\cdot\langle\alpha_s G^2\rangle = (0.14\text{–}0.23)\,\mathrm{GeV}^4$. Concerning the dimension $d=6$ four-quark vacuum condensate our result (52) shows a clear deviation from the vacuum saturation approximation value (14), and is in agreement with e^+e^- results [9, 11–12].

Turning to the axial-vector channel and repeating the above analysis we find first that the duality region in this case is somewhat wider, as may be appreciated from Fig. 5, i.e.

$$1.75\,\mathrm{GeV}^2 \leqq s_0 \leqq 2.25\,\mathrm{GeV}^2 \tag{54}$$

One may understand the result $s_0|_A > s_0|_V$ on account of $M_{A_1} > M_\rho$. With a wider and better duality region one would expect the vacuum condensates to be more stable in s_0, and thus to be affected by a lesser uncertainty. This is indeed the case as shown in Fig. 6. The numerical results now read

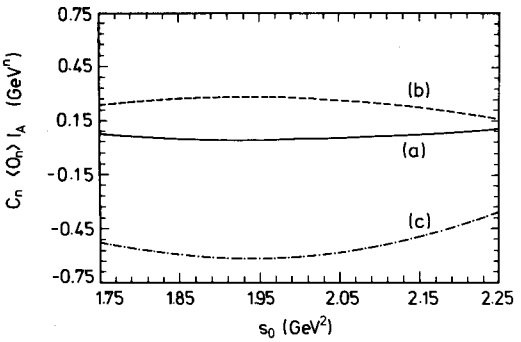

Fig. 6. Behaviour of $C_4\langle O_4\rangle_A$ (curve a), $C_6\langle O_6\rangle_A$ (curve b) and $C_8\langle O_8\rangle_A$ (curve c) as obtained from the FESR (22)–(23) in the axial-vector channel

$$C_4\langle O_4\rangle_A = (0.045 - 0.10)\,\mathrm{GeV}^4 \tag{55}$$

$$C_6\langle O_6\rangle_A = (0.16 - 0.28)\,\mathrm{GeV}^6 \tag{56}$$

and using (12) and (18)

$$\frac{\pi}{3}\langle\alpha_s G^2\rangle = (0.04 - 0.09)\,\mathrm{GeV}^4. \tag{57}$$

It is rewarding that the use of two independent sets of experimental data lead to essentially the same value for the gluon condensate. This is due to the fact that the results we obtain for $C_4\langle O_4\rangle_V$ and $C_4\langle O_4\rangle_A$ satisfy (20). Notice furthermore that $C_6\langle O_6\rangle_A$ has the same sign as expected from theoretical considerations (V.S.), cf. (21), although its value is a factor 2–3 larger than expected from the vacuum saturation approximation.

6. Vacuum condensates from Laplace transform sum rules

First of all we wish to elaborate on the point raised in Sect. 3.4, (ii), concerning the potential bias of Laplace transform determinations of vacuum condensates. Let us concentrate, for instance, on the vector channel and compute $R(\sigma)$ in (29) using the data on the spectral function complemented with the continuum contribution starting at s_0, (49). The result is shown in Fig. 7 (solid curve) for values of σ inside the sum rule window $\sigma \simeq (0.5 - 1.25)\,\mathrm{GeV}^{-2}$. Suppose now that we were to set $C_6\langle O_6\rangle_V = C_8\langle O_8\rangle_V = \cdots = 0$ and fit $C_4\langle O_4\rangle_V$ in (30) so that $R(\sigma)|_{\mathrm{QCD}} \simeq R(\sigma)|_{\mathrm{DATA}}$ e.g. in a chi-squared sense. A very reasonable fit would then be obtained with $C_4\langle O_4\rangle_V = -(0.02 - 0.04)\,\mathrm{GeV}^4$ as shown in Fig. 7 (broken curves). Since on very general grounds [1] $C_4\langle O_4\rangle > 0$ this result is meaningless, in spite of being the best fit to the Laplace ratio (29). Including next $C_6\langle O_6\rangle_V$ in the fit will change $C_4\langle O_4\rangle_V$ and lead to a pair of 'effective' values for these two condensates. These 'effective' values could be the true values if and only if the additional presence of $C_8\langle O_8\rangle_V$ would induce no sizable changes. As we shall argue in Sect. 8 this may well not be the case here. A similar observation has been made recently in [12]. Therefore, in our opinion Laplace transform sum rules should not be used in isolation but rather, in conjunction with other methods (e.g. FESR) to search for overall consistency. In short: they are a necessary but in general not a sufficient condition for consistency.

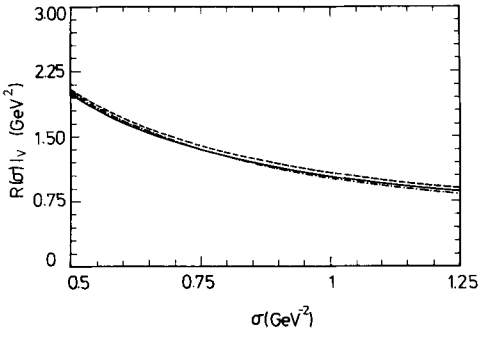

Fig. 7. The solid curve shows the behaviour of the vector Laplace ratio $R(\sigma)|_{\mathrm{DATA}}$. The upper (lower) broken curves correspond to $R(\sigma)|_{\mathrm{QCD}}$ for $C_6\langle O_6\rangle_V = C_8\langle O_8\rangle_V = 0$ and $C_4\langle O_4\rangle_V = -0.04\,\mathrm{GeV}^4$ ($-0.02\,\mathrm{GeV}^4$)

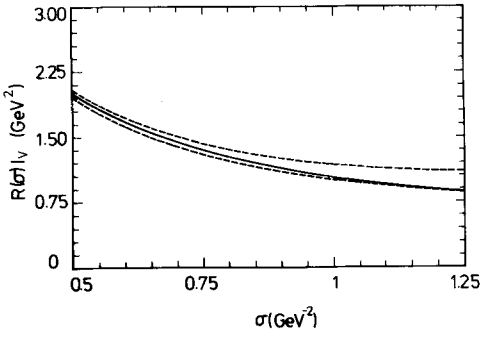

Fig. 8. The solid curve is the same as in Fig. 7. The upper (lower) broken curves correspond to $R(\sigma)|_{\mathrm{QCD}}$ for $C_6\langle O_6\rangle_V = -0.16\,\mathrm{GeV}^6$, $C_8\langle O_8\rangle_V = 0$, and $C_4\langle O_4\rangle_V = 0.025\,\mathrm{GeV}^4$ ($0.11\,\mathrm{GeV}^4$)

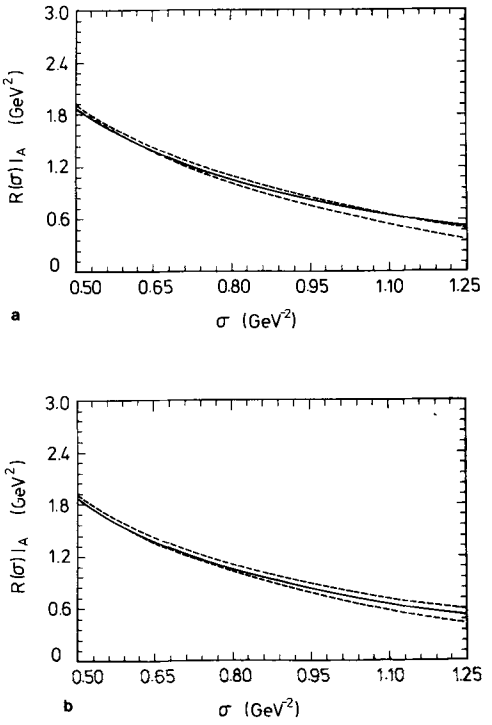

Fig. 9. a The solid curve shows the behaviour of the axial-vector Laplace ratio $R(\sigma)|_{\mathrm{DATA}}$. The upper (lower) broken curves correspond to $R(\sigma)|_{\mathrm{QCD}}$ for $C_4\langle O_4\rangle_A = 0.045\,\mathrm{GeV}^4$, $C_8\langle O_8\rangle_A = 0$ and $C_6\langle O_6\rangle_A = 0.1\,\mathrm{GeV}^6$ ($0.2\,\mathrm{GeV}^6$). **b** The solid curve is the same as in **a**. The broken curves correspond to $R(\sigma)_{\mathrm{QCD}}$ for $C_4\langle O_4\rangle_A = 0.1\,\mathrm{GeV}^4$, $C_8\langle O_8\rangle_A = 0$ and $C_6\langle O_6\rangle_A = 0$($0.1\,\mathrm{GeV}^6$)

Following this philosophy, we have used the values of the condensates determined with FESR to compute $R(\sigma)|_{\mathrm{QCD}}$, (30), and confronted it to $R(\sigma)$ obtained from the data through (29). In Fig. 8 we show $R(\sigma)|_{\mathrm{QCD}}$ in the vector channel for $C_4\langle O_4\rangle_V = 0.025\,\mathrm{GeV}^4$, $C_6\langle O_6\rangle_V = -0.16\,\mathrm{GeV}^6$ (upper broken curve), and $C_4\langle O_4\rangle_V = 0.11\,\mathrm{GeV}^4$, $C_6\langle O_6\rangle_V = -0.16\,\mathrm{GeV}^6$ (lower broken curve), both for $C_8\langle O_8\rangle_V = \cdots = 0$. The solid curve in this figure corresponds to $R(\sigma)|_{\mathrm{DATA}}$. For s_0 we have used values inside the duality region (50). Other combinations of eigenvalue solutions to the FESR lead to equally acceptable results for $R(\sigma)|_{\mathrm{QCD}}$ with the exception of $C_6\langle O_6\rangle_V$ values near the high end of (52). In view of our previous discussion, and since we are neglecting $C_8\langle O_8\rangle_V$, we do not ascribe much significance to this discrepancy.

In Fig. 9a we show $R(\sigma)|_{\mathrm{QCD}}$ in the axial-vector channel for $C_4\langle O_4\rangle_A = 0.045\,\mathrm{GeV}^4$, $C_6\langle O_6\rangle_A = 0.1\,\mathrm{GeV}^6$ (upper broken curve) and $C_6\langle O_6\rangle_A = 0.2\,\mathrm{GeV}^6$ (lower broken curve) together with $R(\sigma)|_{\mathrm{DATA}}$ (solid curve). Using the higher value in (55), i.e. $C_4\langle O_4\rangle_A = 0.1\,\mathrm{GeV}^4$, would require that $C_6\langle O_6\rangle_A \simeq (0 - 0.1)\,\mathrm{GeV}^6$ in order to get agreement with $R(\sigma)|_{\mathrm{DATA}}$, as shown in Fig. 9b. In fact, an almost perfect fit would be obtained if $C_6\langle O_6\rangle_A = 0.05\,\mathrm{GeV}^6$.

However, such a value is well outside the duality range (56).

In summary, with some exceptions the eigenvalue solutions to the FESR satisfy also the Laplace transform QCD sum rules. As noted above, these exceptions correspond to values of $C_6\langle O_6\rangle_V$ near the high end of (52), and to the value $C_4\langle O_4\rangle_A \simeq 0.1\,\text{GeV}^4$ which appears to require a $C_6\langle O_6\rangle_A$ outside the duality range (56). If one had sound theoretical arguments to support the assumption that $C_8\langle O_8\rangle_{V,A}$ is negligible, then this confrontation between FESR and Laplace transform results could be useful to narrow down the range of the predictions. However, we shall argue in Sect. 8 that this does not seem to be the case and, furthermore, that the above discrepancies disappear almost entirely once $C_8\langle O_8\rangle_{V,A}$ is included in $R(\sigma)|_{\text{QCD}}$.

7 Heat evolution tests

In this section we perform the heat evolution tests [10] in order to check if there is duality between the hadronic data and the set of QCD parameters determined previously from the sum rules. To this end we have computed, from (31), (34)–(35) and (49), the

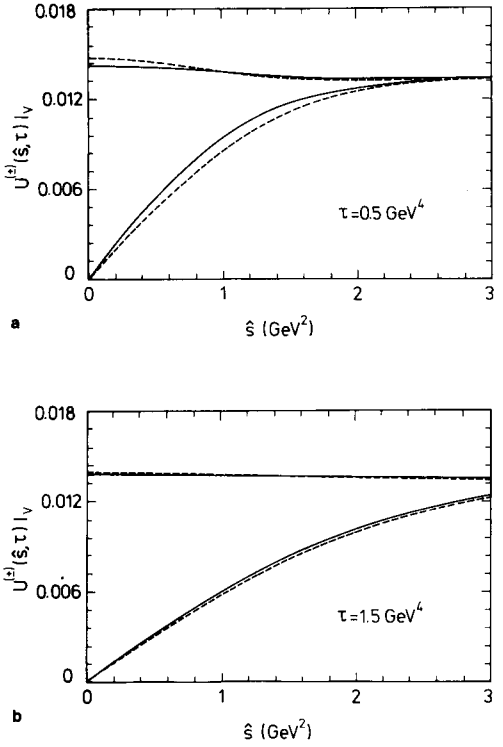

Fig. 10. a The Gaussian transforms $U^+(\hat{s},\tau)|_{\text{DATA}}$ (upper solid curve) and $U^-(\hat{s},\tau)|_{\text{DATA}}$ (lower solid curve), in the vector channel, at a 'time' $\tau = 0.5\,\text{GeV}^4$. The upper broken curve corresponds to $U^+(\hat{s},\tau)|_{\text{QCD}}$ for $C_6\langle O_6\rangle_V = -0.16\,\text{GeV}^6$ and the lower broken curve to $U^-(\hat{s},\tau)|_{\text{QCD}}$ for $C_4\langle O_4\rangle_V = 0.11\,\text{GeV}^4$ and $C_8\langle O_8\rangle_V = 0$. **b** Same as **a** but at a later 'time' $\tau = 1.5\,\text{GeV}^4$. For longer 'times' the corresponding solid and broken curves overlap completely

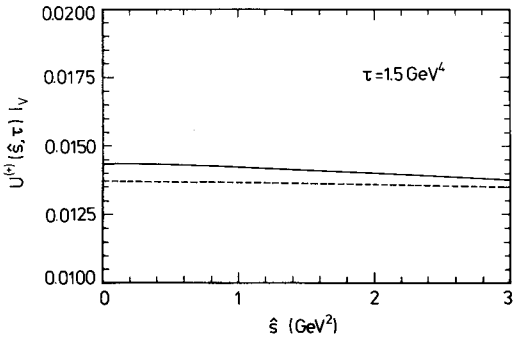

Fig. 11. A comparison between $U^+(\hat{s},\tau)|_{\text{DATA}}$ in the vector channel (solid curve) and $U^+(\hat{s},\tau)|_{\text{QCD}}$ for $C_6\langle O_6\rangle_V = 0$, at $\tau = 1.5\,\text{GeV}^4$

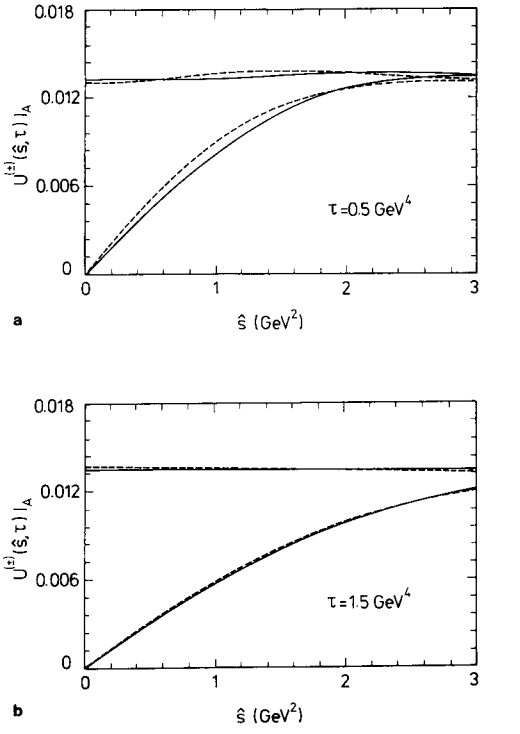

Fig. 12. a The Gaussian transforms $U^+(\hat{s},\tau)|_{\text{DATA}}$ (upper solid curve) and $U^-(\hat{s},\tau)|_{\text{DATA}}$ (lower solid curve) in the axial-vector channel, at a 'time' $\tau = 0.5\,\text{GeV}^4$. The upper broken curve corresponds to $U^+(\hat{s},\tau)|_{\text{QCD}}$ for $C_6\langle O_6\rangle_A = 0.16\,\text{GeV}^6$ and the lower broken curve to $U^-(\hat{s},\tau)|_{\text{QCD}}$ for $C_4\langle O_4\rangle_A = 0.045\,\text{GeV}^4$, $C_8\langle O_8\rangle_A = 0$. **b** Same as **a** but at a later 'time' $\tau = 1.5\,\text{GeV}^4$. For longer 'times' the corresponding solid and broken curves overlap completely

Gaussian transforms $U^{\pm}_{V,A}(\hat{s},\tau)|_{\text{DATA}}$ using the parametrization of the vector and axial-vector spectral functions discussed in Sect. 4, as well as $U^{\pm}_{V,A}(\hat{s},\tau)|_{\text{QCD}}$, (36)–(37), for values of s_0 inside the duality regions (50), (54), and vacuum condensates as in (51), (52), (55) and (56). In Fig. 10a and b we show $U^{\pm}_V(\hat{s},\tau)|_{\text{DATA}}$ (solid curves) together with $U^{\pm}_V(\hat{s},\tau)|_{\text{QCD}}$ (broken curves) for $C_4\langle O_4\rangle_V = 0.11\,\text{GeV}^4$ and $C_6\langle O_6\rangle_V = -0.16\,\text{GeV}^6$, at the two different 'times' $\tau = 0.5\,\text{GeV}^4$ and $\tau = 1.5\,\text{GeV}^4$, respectively. As it may be appreciated from these figures, with increasing 'time' the heat

distribution of the data matches the theoretical heat distribution computed with the above values of the QCD parameters. For later 'times', i.e. $\tau > 1.5\,\mathrm{GeV}^4$, this matching improves to the point that the two curves cannot be distinguished. As an example of a set of QCD parameters which do not pass this test we show in Fig. 11 the function $U_V^+(\hat{s},\tau)|_{\mathrm{QCD}}$ for $C_6\langle O_6\rangle_V = 0$ at $\tau = 1.5\,\mathrm{GeV}^4$. Recall that this case gave a good fit to the Laplace ratio (29) with a negative value of $C_4\langle O_4\rangle_V$ (cf. Sect. 6). Repeating the procedure for other values of the vacuum condensates inside the duality region we find equally good heat evolutions with the exception of $C_6\langle O_6\rangle_V$ values near the high end of (52). A relative qualitative comparison among all possibilities confirms the result (51) but narrows down the range (52) to

$$C_6\langle O_6\rangle_V = -(0.16 - 0.24)\,\mathrm{GeV}^6. \tag{58}$$

Notice that for $\hat{x} \equiv \hat{s}/2\sqrt{\tau}$ large, the vacuum condensates have no practical impact on $U^{\pm}(\hat{s},\tau)$ due to their exponential suppression (cf. eqs. (36)–(37)). In this region of large $\hat{x}$ one is then testing duality between s_0 and perturbative QCD. The rate of approach to the asymptotic limit

$$\lim_{\hat{x}\to\infty} U^{\pm}(\hat{s},\tau) = \frac{1}{8\pi^2} \tag{59}$$

depends, of course, on the value of τ as may be appreciated e.g. from Fig. 10a and b.

Turning to the axial-vector channel, we show in Fig. 12a and b $U^{\pm}(\hat{s},\tau)|_{\mathrm{DATA}}$ together with the corresponding QCD transforms for $C_4\langle O_4\rangle_A = 0.045\,\mathrm{GeV}^4$ and $C_6\langle O_6\rangle_A = 0.16\,\mathrm{GeV}^6$ at the 'times' $\tau = 0.5\,\mathrm{GeV}^4$ and $\tau = 1.5\,\mathrm{GeV}^4$, respectively. Heat evolutions for other values of the condensates in the duality range (55)–(56) were also carried out. They are of comparable good quality and thus confirm the sum rule results.

8 On the value of $C_8\langle O_8\rangle$

In principle the FESR (23) with $N = 1$ may be used to determine the numerical value of $C_8\langle O_8\rangle_{V,A}$. However, given the rather high weight of the spectral function in this case one would expect the accuracy of the results to be somewhat limited. With this due reservation in mind we have solved eq. (23) in the vector and axial-vector channels for values of s_0 inside the duality regions (50) and (54). The results for $C_8\langle O_8\rangle_V$ and $C_8\langle O_8\rangle_A$ are exhibited in Figs. 4 and 6 (curve (c)), respectively. Numerically they read

$$C_8\langle O_8\rangle_V = (0.28 - 0.55)\,\mathrm{GeV}^8 \tag{60}$$

$$C_8\langle O_8\rangle_A = -(0.36 - 0.54)\,\mathrm{GeV}^8. \tag{61}$$

As with $C_4\langle O_4\rangle$ and $C_6\langle O_6\rangle$, the result for $C_8\langle O_8\rangle$ in the axial-vector channel is more stable and less inaccurate than that in the vector channel. This is a reflection of the quality of the corresponding duality regions as may be appreciated from Figs. 3 and 5. To remain on the safe side we proceed with our discussion choosing the lowest eigenvalue in (60)–(61).

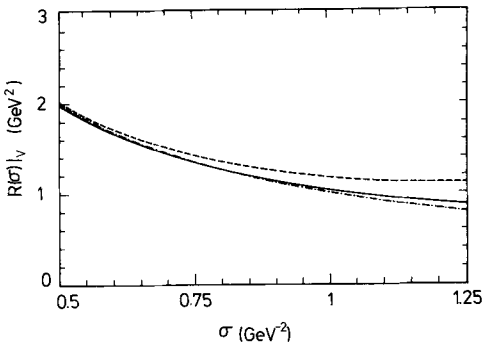

Fig. 13. The Laplace ratio $R(\sigma)|_{\mathrm{DATA}}$ in the vector channel (solid curve) compared to $R(\sigma)|_{\mathrm{QCD}}$ for $C_4\langle O_4\rangle_V = 0.025\,\mathrm{GeV}^4$, $C_6\langle O_6\rangle_V = -0.16\,\mathrm{GeV}^6$, $C_8\langle O_8\rangle_V = 0$ (upper broken curve) and $C_8\langle O_8\rangle_V = 0.25\,\mathrm{GeV}^8$ (lower broken curve)

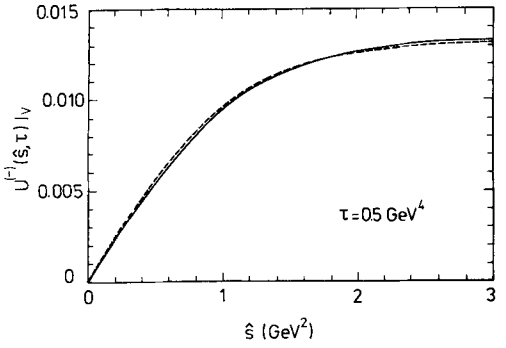

Fig. 14. The Gaussian transform $U^-(\hat{s},\tau)|_{\mathrm{DATA}}$ in the vector channel (solid curve) and $U^-(\hat{s},\tau)|_{\mathrm{QCD}}$ for $C_4\langle O_4\rangle_V = 0.025\,\mathrm{GeV}^4$ and $C_8\langle O_8\rangle_V = 0.28\,\mathrm{GeV}^8$, at $\tau = 0.5\,\mathrm{GeV}^4$

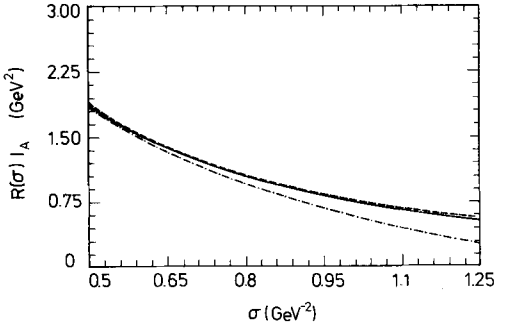

Fig. 15. The Laplace ratio $R(\sigma)|_{\mathrm{DATA}}$ in the axial-vector channel (solid curve) compared to $R(\sigma)|_{\mathrm{QCD}}$ for $C_4\langle O_4\rangle_A = 0.045\,\mathrm{GeV}^4$, $C_6\langle O_6\rangle_A = 0.28\,\mathrm{GeV}^6$, $C_8\langle O_8\rangle_A = 0$ (lower broken curve) and $C_8\langle O_8\rangle_A = -0.36\,\mathrm{GeV}^8$ (upper broken curve)

In order to show the influence of $C_8\langle O_8\rangle$ on the Laplace analysis we plot in Fig. 13 $R(\sigma)|_{\mathrm{DATA}}$ (solid curve) and $R(\sigma)|_{\mathrm{QCD}}$ for $C_4\langle O_4\rangle_V = 0.025\,\mathrm{GeV}^4$, $C_6\langle O_6\rangle_V = -0.16\,\mathrm{GeV}^6$, $C_8\langle O_8\rangle_V = 0$ (upper broken curve), and $C_8\langle O_8\rangle_V = 0.28\,\mathrm{GeV}^8$ (lower broken curve). The agreement between the theoretical and the experimental Laplace ratios is clearly im-

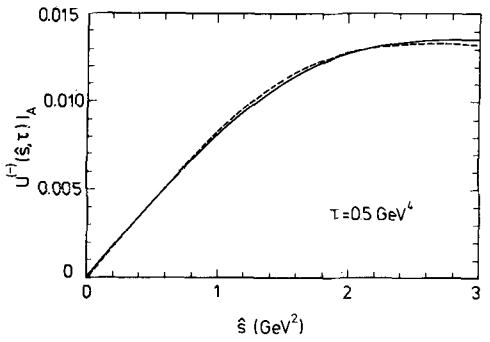

Fig. 16. The Gaussian transform $U^-(\hat{s},\tau)|_{\text{DATA}}$ in the axial-vector channel (solid curve) and $U^-(\hat{s},\tau)|_{\text{QCD}}$ for $C_4\langle O_4\rangle_A = 0.045\,\text{GeV}^4$, $C_8\langle O_8\rangle_A = -0.36\,\text{GeV}^8$, at $\tau = 0.5\,\text{GeV}^4$

proved by the presence of $C_8\langle O_8\rangle_V$. Concerning the heat evolution tests, a remarkable amelioration of the matching between $U_V^-(\hat{s},\tau)|_{\text{QCD}}$ and $U_V^-(\hat{s},\tau)|_{\text{DATA}}$ is achieved, already at early 'times', when one includes the contribution from $C_8\langle O_8\rangle_V$, as seen from Fig. 14 for $\tau = 0.5\,\text{GeV}^4$. The good agreement found earlier between $U_V^-(\hat{s},\tau)|_{\text{DATA}}$ and $U_V^-(\hat{s},\tau)|_{\text{QCD}}$ (with $C_8\langle O_8\rangle_V = 0$) at later 'times', e.g. $\tau = 1.5\,\text{GeV}^4$, is less affected by $C_8\langle O_8\rangle_V$ on account of the τ-suppression (see (37)).

Similar improvements take place in the axial-vector channel as may be appreciated from Fig. 15 where $R(\sigma)|_{\text{QCD}}$ has been computed using $C_4\langle O_4\rangle_A = 0.045\,\text{GeV}^4$, $C_6\langle O_6\rangle_A = 0.28\,\text{GeV}^6$, $C_8\langle O_8\rangle_A = 0$ (lower broken curve) and $C_8\langle O_8\rangle_A = -0.36\,\text{GeV}^8$ (upper broken curve). In Fig. 16 we show $U_A^-(\hat{s},\tau)|_{\text{DATA}}$ at $\tau = 0.5\,\text{GeV}^4$ (solid curve) compared with $U_A^-(\hat{s},\tau)|_{\text{QCD}}$ for $C_4\langle O_4\rangle_A$ as above and $C_8\langle O_8\rangle_A = -0.36\,\text{GeV}^8$. This overall improvement caused by the inclusion of $C_8\langle O_8\rangle$, as calculated from FESR, in the Laplace and Gaussian transforms should not come as a surprise if one keeps in mind that FESR follow from the latter.

In addition to what has just been pointed out, the rather large values of $C_8\langle O_8\rangle_{V,A}$ derived through FESR may have important phenomenological consequences in applications of QCD sum rules to other channels. To see how much the results (60)–(61) deviate from current theoretical estimates let us concentrate first on the vector channel. The pure gluonic piece of $C_8\langle O_8\rangle_V$, as calculated in [24], can be casted as follows

$$C_8\langle O_8\rangle_V|_{\text{gluons}} = \tfrac{1}{324}[-4\langle\hat{O}_1\rangle - 196\langle\hat{O}_2\rangle - 292\langle\hat{O}_3\rangle + 540\langle\hat{O}_4\rangle] \tag{62}$$

where

$$\hat{O}_1 = g^4\,\text{Tr}(\hat{G}_{\mu\nu}\hat{G}_{\mu\nu}\hat{G}_{\alpha\beta}\hat{G}_{\alpha\beta}) \tag{63}$$

$$\hat{O}_2 = g^4\,\text{Tr}(\hat{G}_{\mu\nu}\hat{G}_{\alpha\beta}\hat{G}_{\mu\nu}\hat{G}_{\alpha\beta}) \tag{64}$$

$$\hat{O}_3 = g^4\,\text{Tr}(\hat{G}_{\mu\nu}\hat{G}_{\nu\alpha}\hat{G}_{\alpha\beta}\hat{G}_{\beta\mu}) \tag{65}$$

$$\hat{O}_4 = g^4\,\text{Tr}(\hat{G}_{\mu\nu}\hat{G}_{\alpha\beta}\hat{G}_{\nu\alpha}\hat{G}_{\beta\mu}) \tag{66}$$

with

$$\hat{G}_{\mu\nu} \equiv G^a_{\mu\nu}\frac{\lambda^a}{2}. \tag{67}$$

A reference estimate of (62) may be obtained using the vacuum saturation approximation [1, 36] in which case

$$C_8\langle O_8\rangle_V|^{\text{V.S.}}_{\text{gluons}} \simeq -\mathcal{O}(10^{-3} - 10^{-2})\,\text{GeV}^8 \tag{68}$$

where (53), (57) were used. However, it should be kept in mind that there are no theoretical arguments to support this approximation [37–38] and, in fact, some authors have claimed deviations of up to factors of ten [37, 39]. In any case, notice that even the sign of (68) disagrees with the FESR result (60). The huge factor needed to reconcile (68) with (60), though, does not necessarily translate into huge deviations from vacuum saturation for the individual matrix elements $\langle\hat{O}_{1-4}\rangle$ as these appear in the combination (62). As easily checked, it would be enough to admit e.g. individual mild deviations, but with appropriate signs, to recover (60).

The most serious problem lies in the relative sign difference between (60) and (61), as the pure gluonic contributions to $C_8\langle O_8\rangle$ should be the same in the vector and axial-vector channels. This may be an indication that the contribution from the other operators which appear in the complete expression for $C_8\langle O_8\rangle$, usually assumed to be non-leading, might be important. There are, in fact, three additional operators involving gluon fields together with the source current $j^a_\mu \equiv D_\mu G^a_{\alpha\mu}$, as well as ten quark operators. Although the Wilson coefficients for the vector case have been computed in [24] this is not enough as there are not even theoretical estimates for many of these matrix elements.

The values of the $d = 8$ vacuum condensates (60)–(61) are, of course, meant to be the complete result, i.e. they include the contribution from all possible 17 operators. In view of their stability in s_0 and of the improvement achieved in the Laplace sum rules as well as in the heat evolution tests, both for the vector and axial-vector channels, we feel that these results should be reliable to some reasonable extent.

9 Conclusions

Available experimental data on semileptonic decays of the τ-lepton, $\tau \to \nu_\tau + n\pi$, allows for a determination of the vector and axial-vector spectral functions (cf. Sect. 4). This information has been used here in order to extract the values of the leading vacuum condensates appearing in the Operator Product Expansion of current correlators. Our technical procedure was based on a combined use of FESR, Laplace and Gaussian transform QCD sum rules. In this fashion we have been able to perform valuable consistency checks and verify explicitly the duality interplay

Table 1. Results of our combined analysis using FESR Laplace and Gaussian transform QCD sum rules

QCD parameter	Vector channel	Axial-vector channel	Standard value
s_0 (GeV^2)	1.44–1.71	1.75–2.25	—
$C_4\langle O_4\rangle$ (GeV^4)	0.025–0.11	0.045–0.10	0.03
$(\pi/3)\langle\alpha_s G^2\rangle$ (GeV^4)	0.03–0.12	0.04–0.09	0.04
$C_6\langle O_6\rangle$ (GeV^6)	$-$(0.16–0.24)	0.16–0.28	-0.06 (vector)$\vert_{\text{V.S.}}$ 0.09 (axial)$\vert_{\text{V.S.}}$
$C_8\langle O_8\rangle$ (GeV^8)	0.28–0.55	$-$(0.36–0.54)	—

between the hadronic data and the QCD parameters so determined. In Table 1 we collect our results and show the standard values (3), (14) and (21) for comparison. It is rewarding to find that the use of two independent sets of experimental data lead to essentially the same result for the gluon condensate. The latter is consistent with the standard value (3) as well as with higher values derived from e^+e^- data [11–12] and other sources [2, 6, 13–14], but it is barely consistent with a recent s-wave charmonium determination [7]. Our value for the dimension $d=6$ four-quark condensate $C_6\langle O_6\rangle_V$, though, indicates a clear deviation from the standard vacuum saturation approximation, in agreement with earlier claims [9, 11–12, 15–17]. On the other hand, our result for $C_6\langle O_6\rangle_A$ has the same sign as expected from theoretical considerations (V.S.), cf. (21), but its value shows also a sizable deviation from vacuum saturation (for a lucid and detailed presentation of the vacuum saturation approximation see [40]).

We have also determined $C_8\langle O_8\rangle_{V,A}$ using FESR and found that its inclusion in the Laplace and Gaussian transforms leads to an improved duality between QCD and the data. However, in view of the rather high weight of the spectral function one should not expect the same level of accuracy as for lower dimensional condensates. In any case, we find a clear sign difference between $C_8\langle O_8\rangle_V$ and $C_8\langle O_8\rangle_A$, which is also supported by the stability of the results. This could be an indication that the pure four-gluon operator contributions to $C_8\langle O_8\rangle$ may not be leading. In view of its potential phenomenological consequences, this possibility deserves a separate theoretical study which is, however, beyond the scope of this paper.

Acknowledgements. The authors are indebeted to D. Broadhurst, B. Guberina, N. Paver and R.D. Peccei for very helpful discussions, and to the ARGUS collaboration for making their τ-lepton distributions available to them. One of us (C.A.D.) wishes to thank R.A. Bertlmann, M. Perrottet and E. de Rafael for sharing their knowledge on QCD sum rules.

References

1. M.A. Shifman, A.I. Vainshtein, V.I. Zakharov: Nucl. Phys. B147, (1978) 385, 448, 519
2. L.J. Reinders, H. Rubinstein, S. Yazaki: Phys. Rep. 127 (1985) 1
3. V.A. Novikov, M.A. Shifman, A.I. Vainshtein, V.I. Zakharov: Nucl. Phys. B191 (1981) 301
4. L.J. Reinders, H.R. Rubinstein, S. Yazaki: Nucl. Phys. B186 (1981) 109; Phys. Lett. 138B (1984) 425
5. B. Guberina, R. Meckbach, R.D. Peccei, R. Rückl: Nucl. Phys. B184 (1981) 476
6. S.N. Nikolaev, A.V. Radyushkin: Sov. J. Nucl. Phys. 39 (1984) 91
7. J. Marrow, G. Shaw: Z. Phys. C—Particles and Fields 33 (1986) 237
8. S.I. Eidelman, L.M. Kurdadze, A.I. Vainshtein: Phys. Lett. 82B (1979) 278
9. G. Launer, S. Narison, R. Tarrach: Z. Phys. C—Particles and Fields 26 (1984) 433
10. R.A. Bertlmann, G. Launer, E. de Rafael: Nucl. Phys. B250 (1985) 61
11. R.A. Bertlmann et al.: CERN Report No. CERN-TH-4898 (1987); R.A. Bertlmann in: Proceedings of the XVII International Symposium on Multiparticle Dynamics. M. Markytan, W. Majerotto, J. Mac Naughton, (eds.) Singapore: World Scientific 1987; C.A. Dominguez: DESY Report No. DESY-87-002 (1987); in: Quarks, gluons and hadronic matter; R. Viollier, N. Warner, (eds.). Singapore: World Scientific 1987.
12. J. Bordes, V. Gimenez, J.A. Peñarrocha: Universität Mainz Report (1987)
13. J.S. Bell, R.A. Bertlmann: Nucl. Phys. B177 (1981) 218; B187 (1981) 285; Phys. Lett. 137B (1984) 107
14. P. Ditsas, G. Shaw: Phys. Lett. 106B (1981), 336; Nucl. Phys. B229 (1983) 29; A. Bradley, C.S. Langensiepen, G. Shaw: Phys. Lett. 102B (1981) 180, 359
15. M. Kremer, N.A. Papadopoulos, K. Schilcher: Phys. Lett. 143B (1984) 476
16. Y. Chung, H.G. Dosch, M. Kremer, D. Schall: Z. Phys. C—Particles and Fields 25 (1984) 151
17. H.G. Dosch, in: Proceedings of the Workshop on Non-Perturbative Methods. S. Narison (ed.) Singapore: World Scientific 1986
18. H. Albrecht et al.: Z. Phys. C—Particles and Fields 33 (1986). 7; A. Golutvin and U. Binder: private communication
19. R.D. Peccei, J. Solá: Nucl. Phys. B281 (1987) 1
20. E. de Rafael, in: Quantum chromodynamics. Proceedings of the X G.I.F.T. International Seminar on Theoretical Physics, Jaca, Huesca (Spain), Lecture Notes in Physics No. 118, T. Heidelberg, New York: J.L. Alonso R. Tarrach (eds.) Berlin Springer 1980)
21. M. Dine, J. Sapirstein: Phys. Rev. Lett. 43 (1979), 668; K.C. Chetyrkin, A.L. Kataev F.V. Tkachov: Phys. Lett. 85B (1979) 277; W. Celmaster, R.J. Gonsalves: Phys. Rev. Lett. 44 (1980) 560; Phys. Rev. D21 (1980) 3312
22. M.S. Dubovikov, A.V. Smilga: Nucl. Phys. B185 (1981) 109
23. W. Hubschmid, S. Mallik: Nucl. Phys. B207 (1982) 29
24. D.J. Broadhurst, S.C. Generalis: Phys. Lett. 165B (1985) 175
25. H. Pagels: Phys. Rep. C16 (1975) 219
26. C.A. Dominguez, M. Kremer, N. Papadopoulos, K. Schilcher: Z. Phys. C—Particles and Fields 27 (1985) 481
27. C.A. Dominguez, E. de Rafael: Ann. Phys. (N.Y.) 174 (1987) 372
28. A. Pich, E. de Rafael: Phys. Lett. 158B (1985) 477
29. C.A. Dominguez, N. Paver: Z. Phys. C—Particles and Fields 31 (1986), 591; 32 (1986) 391
30. S. Narison, E. de Rafael: Phys. Lett. 103B (1981) 57
31. G. Launer: Z. Phys. C—Particles and Fields 32 (1986) 557
32. F.J. Gilman, S.H. Rhie: Phys. Rev. D31 (1985) 1066
33. B.C. Barish, R. Stroynowski: Caltech Report No. CALT-68-1425 (1987) (Submitted to Phys. Rep.)
34. W. Ruckstuhl et al.: Phys. Rev. Lett. 56 (1986) 2132
35. Particle Data Group: Phys. Lett. 170B (1986) 1
36. V.A. Novikov, M.A. Shifman, A.I. Vainshtein, V.I. Zakharov: Nucl. Phys. B165 (1980) 67
37. E.V. Shuryak: Nucl. Phys. B203 (1982) 93, 116, 140
38. V.A. Novikov, H.A. Shifman, A.I. Vainshtein, V.I. Zakharov: Nucl. Phys. B237 (1984) 525
39. M. Müller–Preussker: Phys. Lett. 122B (1983) 165
40. S.C. Generalis, Ph.D. Thesis: Open University Report No. OUT-4102-13 (1984)